crystals

MDPI

Article

Crystal Structure of New Zinc-Hydroxy-Sulfate-Hydrate $Zn_4(OH)_6SO_4 \cdot 2–2.25H_2O$

Tsveta Stanimirova [1,*], Rositsa Nikolova [2] and Nadia Petrova [2]

[1] Department of Mineralogy, Petrology and Economic Geology, Faculty of Geology and Geography, Sofia University "St. Kliment Ohridski", 15 Tzar Osvoboditel Blvd., 1000 Sofia, Bulgaria
[2] Institute of Mineralogy and Crystallography—Bulgarian Academy of Sciences, 107 Acad. G. Bonchev Str., 1113 Sofia, Bulgaria; rosica.pn@clmc.bas.bg (R.N.); nadia5@mail.bg (N.P.)
* Correspondence: stanimirova@gea.uni-sofia.bg; Tel.: +359-878-249-644

Abstract: A theoretical model of the crystal structure of the newly obtained compound $Zn_4(OH)_6SO_4 \cdot 2–2.25H_2O$ based on the compilation of the crystal–chemical properties of two known zinc-hydroxy-sulfate phases—mineral namuwite and hemihydrate—is proposed. The single XRD data confirmed the model and determined the structure, with a trigonal symmetry SG of P-3, the unit cell with a = 8.3418(15) Å and c = 17.595(7) Å, and a cell volume of 1060.3(6) $Å^3$, with Z = 2. The results show that the $Zn_4(OH)_6SO_4 \cdot 2–2.5H_2O$ crystal structure consists of an alternating paired octahedral–tetrahedral doubly decorated hydroxide layer with cationic vacancies and an aqueous interlayer.

Keywords: crystal structure; new Zn-hydroxy sulfate; mixed-layer structure

Citation: Stanimirova, T.; Nikolova, R.; Petrova, N. Crystal Structure of New Zinc-Hydroxy-Sulfate-Hydrate $Zn_4(OH)_6SO_4 \cdot 2–2.25H_2O$. *Crystals* **2024**, *14*, 183. https://doi.org/10.3390/cryst14020183

Academic Editors: Sławomir Grabowski, Shujun Zhang, Jesús Sanmartín-Matalobos and Heike Lorenz

Received: 22 December 2023
Revised: 25 January 2024
Accepted: 27 January 2024
Published: 12 February 2024

1. Introduction

The main reason for the diversity of hydroxy salt mineral species is the binary nature of their structures—they are built up of structural units (SUs) characterized by strong, relatively homogeneous bonds between the components and interstitial complexes (ICs), which weakly bind the structural units to build a three-dimensional crystal structure [1]. The bipolar character of the dominant in the hydroxy salt hydroxyl (OH-) anion predisposes the polymerization of cation–OH polyhedrons (octahedra, tetrahedra, and squares) in one or, more often, two directions. These OH-specific characteristics lead to the formation of SUs in the form of hydroxide layers, chains, and single or coupled ribbons of polyhedra. The diversity of SUs and ICs, and their mutual interactions, predetermine the variety of the 3D arrangements of these structural units and the consequent formation of several minerals [2]. Such a mode of formation also implies the possibility of structural changes in compounds with the same or similar chemical compositions. The different phases can transform into each other, and the study of the mechanisms of these transformations provides a basis for predicting new phases or new conditions for the formation of known phases [3–8].

Recently, we performed a detailed study of the anionic exchange and mutual transformations of Zn-hydroxy salts with the general formula $Zn^{2+}(OH)_{2-x}(A^{n-})_{x/n} \cdot mH_2O$, where A^{n-} is an anion with a charge of n^- (Cl^-, NO_3^-, SO_4^{2-}, and CO_3^{2-}). A crystalline phase with a powder diffraction pattern not described in the International Crystallographic Diffraction Data (ICDD) databases was obtained [9]. A phase with an identical powder X-ray diffraction pattern was also obtained by Maruyama et al. [4,10] during the exchange reaction of gordaite. These authors attributed the increase in the value of the d-spacing of the first reflection to a higher water content in the interlayer space caused by the high hydration ability of the newly incorporated interlayer lithium and calcium cations. Unfortunately, in these two papers, there was no evidence for the presence of cations or the increased content of water molecules in the interlayer space. On the contrary, based on the chemical and thermal decomposition data, we showed that the interlayer water content

is lower ($Zn_4(OH)_6SO_4 \cdot 2–2.25H_2O$) than the initial compounds, besides the processes of this new phase synthesis (during the transformation, the reaction of Zn-hydroxy nitrates with sulfate solutions; Zn-hydroxy sulfates with nitrate solutions; the exchange reaction of Zn-hydroxy sulfate samples (osakaite, namuwite, and gordaites) with alkali iodides) [9].

2. Materials and Methods

2.1. Obtaining a New Phase

From the three different methods of the synthesis of the new phase (the reaction of Zn-hydroxy nitrates with sulfate solutions; the interaction of Zn-hydroxy sulfates with nitrate solutions; the reaction of Zn-hydroxy sulfate samples with alkali iodides) described in the literature [9], in the present study, the synthesis for obtaining the new phase from the interaction of Zn-hydroxy sulfates with NaI was followed. The starting material—a synthetic analog of the mineral namuwite—was obtained by the alkalization of a 1 M $ZnSO_4$ solution to a pH of 6.5 with solid urea. The reaction was held at 95 °C and continuous stirring with a magnetizing stirrer. An amount of 0.5 g of prepared namuwite was dispersed in a 5 mL 1 M solution of NaI. The reaction duration was one to three days. The products were washed with distilled water, filtered, and air-dried for 24 h or at 30 °C for 2 h. The experiments of the synthesis and transformation exchange were repeated at least twice. All experiments were performed with analytical-grade chemicals.

2.2. Methods

All materials were investigated and characterized by powder X-ray diffraction (PXRD), scanning electron microscopy (SEM) coupled with an energy dispersive spectrometer (EDS), Fourier transform infrared spectroscopy (FTIR), differential thermal analyses and thermogravimetry with mass-spectroscopy (DSC-TG-MS), and single-crystal XRD analysis.

The powder XRD patterns were recorded on the D8 Advance Bruker diffractometer. Filtered Cu-Kα radiation was used in the range 2Θ 2–80°, with a step of 0.01° 2Θ, and an exposure time per step of 6.5 s for the starting material and the new phase. The XRD pattern (2Θ 4–80°) of the other samples were obtained with Co-Kα radiation (a step of 0.02° 2Θ, 1.5 s per step). The specialized software Diffrac.Eva (5.2.0.5. version) was used for the qualitative and semiquantitative phase composition determination.

The SEM investigations and chemical analysis were performed by an SEM fitted with an EDS—the apparatus was the JEOL, model JSM-6010PLUS/LA, with a 20 kV accelerating voltage and a spot size of 65 nm.

The infrared spectra were recorded by a Tensor 37 Fourier transform infrared (FTIR) Bruker spectrometer in the spectral region of 400–4000 cm^{-1}. The spectra were collected at room temperature on the samples prepared by the standard KBr pallet technique after N_2-purging and with a spectral resolution of 4 cm^{-1} after averaging over 72 scans.

The DSC-TG-MS were carried out on the DSC-TG analyzer SETSYS2400, SETARAM, at the following conditions: a temperature range from 20 to 1000 °C, in a static air atmosphere, with a heating rate of 10 °C min^{-1}, and 15 mg sample weight. The simultaneous analysis of the evolved gases was performed via mass spectrometry using an OmniStar mass spectrometer connected to the TG apparatus. The intensities related to the main m/z value of the following volatiles, H_2O (18), O_2 (32), and SO_2 (64), were examined.

Single-crystal diffraction data collections were performed by the ω-scan technique on an Agilent Diffraction SuperNova Dual four-circle diffractometer equipped with an Atlas CCD detector using mirror-monochromatized MoKα radiation from the microfocus source (λ = 0.7107 Å).

3. Results and Discussion

3.1. Characterization of the Starting Materials and the Choice of the Structural Model

Data from the powder XRD analysis of the starting material showed that it consisted of namuwite (Figure 1a). After the treatment of the starting namuwite, the SEM and EDS

data showed the preservation of the layered crystal shape and the chemical composition without the presence of additional ions, such as Na or I.

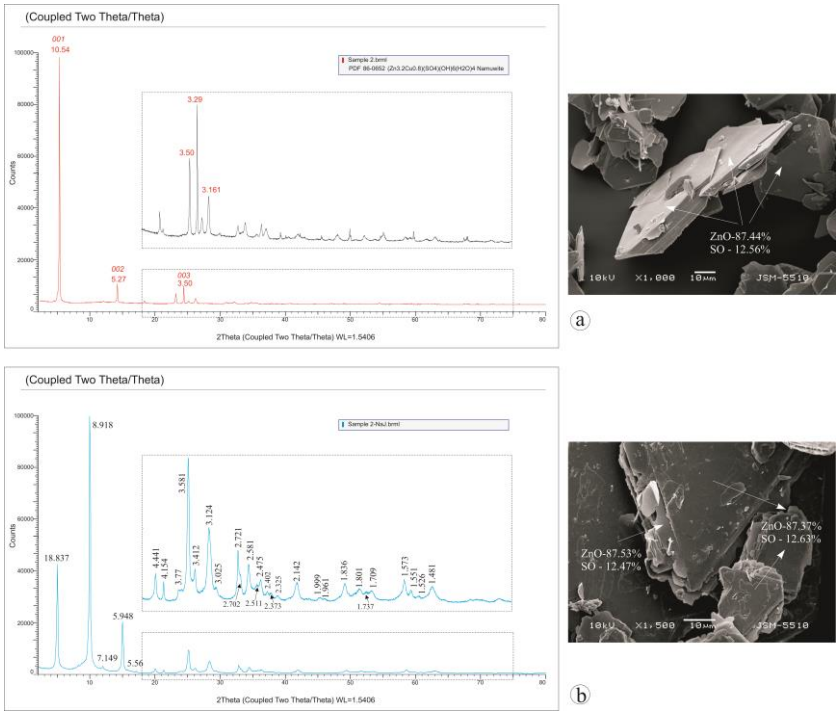

Figure 1. Powder XRD pattern and SEM micrographs of: (**a**) the products obtained by the alkalization of $ZnSO_4$; (**b**) the product after the NaI treatment.

The obtained powder XRD data (interplanar distances and intensities) did not match any phase collected in crystallographic databases or crystallographic open data (COD) and powder diffraction files (PDF-2) (Figure 1b). The powder diffraction data of the "new phase" revealed that the obtained phase owned an interplanar distance of the first reflection of d = 17.84 Å larger that of the starting phase (d_{001} = 10.54 Å) (Figure 1b). Since this reflection was in multiple dependence with the reflections 8.92 Å and 5.95 Å, it can be assumed that they are harmonic reflections. The observed fine–flaky nature of the crystals (Figure 1) implies that these reflections are orders of planar networks of the 00l type. Since the established ratio of ZnO:SO = 6:9 is identical to that of the minerals and their dehydrated phases with the formula $Zn_4(OH)_6SO_4.nH_2O$, it can be assumed that, like other Zn-hydroxy salt minerals, the structure consists of hydroxide layers with cation vacancies [11–18]. The hydroxide layer $[Zn_6\square(OH)_{12}O_2]^{4-}$ is described as a brucite-like layer in which one-seventh of the octahedral sites are vacant and one-seventh of the OH places are occupied by oxygen atoms from SO_4 groups. Above the vacant octahedra on both sides of the layer are placed Zn tetrahedra, made up of three OH groups of the octahedral layer and an apical position occupied by a water molecule. This structural arrangement allows us to describe the octahedral–tetrahedral layer as an "interrupted decorated sheet" [1] (Figure 2).

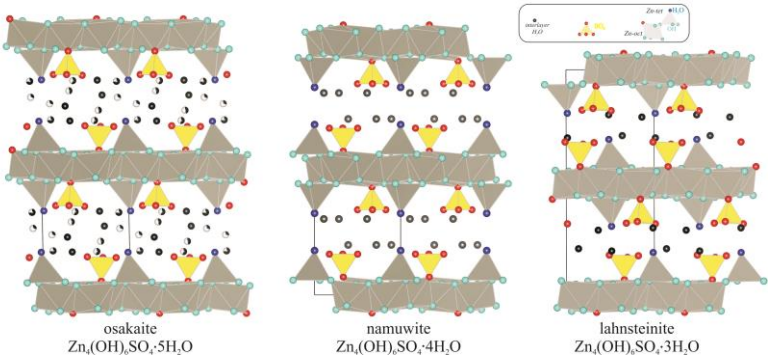

Figure 2. Crystal structures of osakaite according to [13], namuwite according to [10], and lahnshteinite according to [14].

In addition to the established morphological and chemical similarities, the basis for such an assumption is also the observed X-ray reflections with d-spacings of 4.17 Å, 2.72 Å, and 1.57 Å, which are characteristic lines of the hk0 (110, 210, 140) of minerals with this type of structure [5,10,13] and of products of their dehydration [11,12,14], which increase their intensity in untextured preparations (Figure 3). The main difference is in the direction of the ***c*** parameter, where the value of the first reflection with d_{001} is significantly larger than that of the known differently hydrated phases. The parameter ***c*** reflects the layer thickness and the height of the interlayer space, manifested by a gradual decrease in the value of d_{001} in the differently dehydrated phases (Figure 2, Table 1).

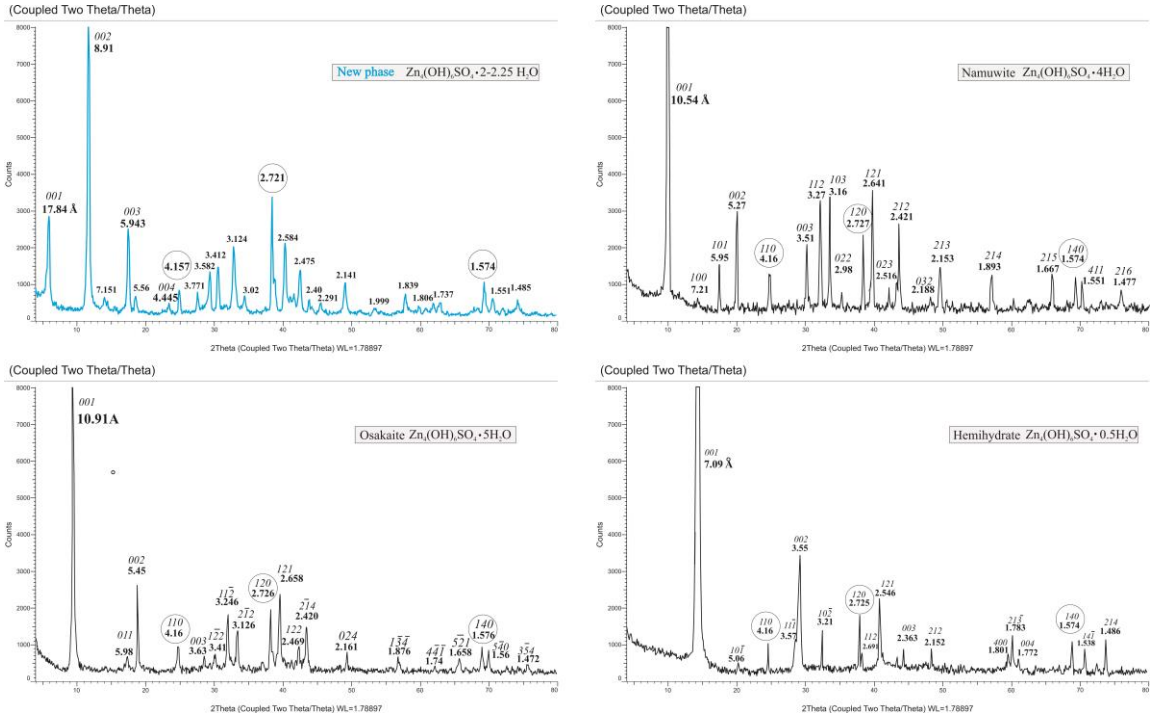

Figure 3. Powder XRD patterns of the disordered (without texture) samples of the new phase, osakaite, namuwite, and hemihydrate.

Table 1. Interplanar distance of d_{001} for differently hydrated $Zn_4(OH)_6SO_4.nH_2O$.

Mineral/Phase	Formula	d_{001}, Å *
osakaite	$Zn_4(OH)_6SO_4 \cdot 5H_2O$	10.90
namuwite	$Zn_4(OH)_6SO_4 \cdot 4H_2O$	10.54
lahnsteinite	$Zn_4(OH)_6SO_4 \cdot 3H_2O$	9.30
dihydrate	$Zn_4(OH)_6SO_4 \cdot 2H_2O$	8–7.4
monohydrate	$Zn_4(OH)_6SO_4 \cdot 1H_2O$	7.23
hemihydrate	$Zn_4(OH)_6SO_4 \cdot 0.5H_2O$	7.09

* Data according to [14,18–20].

Data from the DSC-TG analysis of the studied sample (Figure 4) showed a water content of 2.25 H_2O, in agreement with the data published in the literature for the new phase samples obtained by different synthesis conditions [9]. The obtained H_2O amount of 2–2.25 is too low to cause an increase in the ***c*** parameter to 17.8 Å. One possibility for the observed value could be a polytypic variety of one of the known phases. The measured values of the 00l reflections do not correspond to, or are not multiples of, the d_{001} values of the known phases, which minimizes the probability that the new phase is a polytype of one of the phases. On the other hand, the determined water content of 2–2.25 H_2O suggests that the new phase should be a polytype of the dihydrate phase resulting from the thermal decomposition of the higher hydrated phases [9,14]. For the dihydrate, however, Bear and coauthors [12] were the first to report that there was no discrete value of d_{001}, i.e., the position of the interlayer water molecules was not fixed and constant, which was expressed in a broad peak with a "floating" value of d_{001} in the range 7.4–8 Å [13,14].

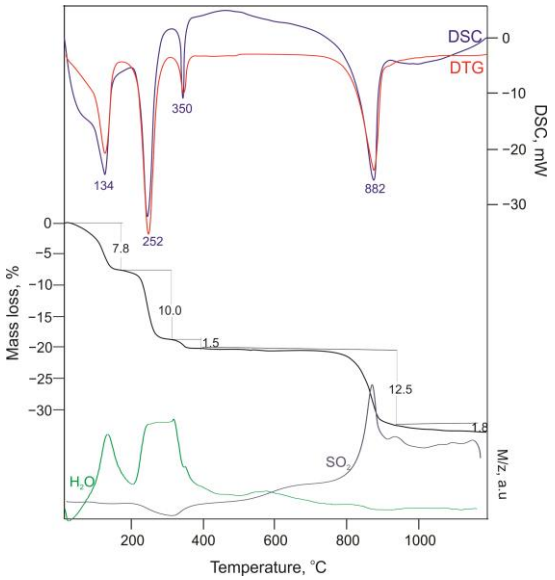

Figure 4. DSC-TG-MS data for the new phase.

Another possibility to explain the value of d_{001} = 17.84 Å is a mixed-layer structure, which is inherent to layered structures [21]. The values of d_{001} of all phases (Table 1) show that there are two variants in which $d_{001} \approx 17.8$ Å of the "new phase" will be obtained through the alternating namuwite and monohydrate package (layer + interlayer) (10.54 + 7.23 = 17.77 Å) and a namuwite and hemihydrate package (10.54 + 7.09 = 17.63 Å). It is known from the literature that monohydrate in a moist environment rehydrates to higher hydrate phases [14], which is not the case.

The stability of the structure and the features of the hemihydrate structure suggest that the combination of the hemihydrate and namuwite pack is realized. The structure of the hemihydrate probably consists of brucite-like sheets of an edge-sharing octahedral with a vacant site position, where the apical oxygen of the tetrahedrally coordinated Zn atom is shared with the Zn tetrahedral from the adjacent layer (like the layer arrangement in

the bechererite structure [22,23]). In this way, the interlayer space is occupied by diortho-connected Zn tetrahedra from two adjacent layers, which prevents its opening and fixes a constant height value.

In the FTIR spectra of the new phase, absorption bands characteristic of the namuwite and hemihydrate structures are registered. Similar to the namuwite structure, the spectra of the new phase present bands in the long-wave range (900–400 cm^{-1}) attributed to the Zn^{2+}–O (O atoms from (OH and SO_4 groups)) interaction, the stretching mode (3400 cm^{-1}) of the hydroxyl groups (a bending mode of about 1634 cm^{-1}), and the bands (1610–1627 cm^{-1}) attributed to the interlayer H_2O molecules (Figure 5a,b). The SO_4 group absorption bands are like the bands of namuwite and hemihydrate (Figure 5c). The topological symmetry of the sulfate group in the namuwite structure is C_{3v} for the monodentate bonding (grafting) in the octahedral layer, manifested by the splitting of ν_3 centered on 1000 cm^{-1} into two bands—at higher and lower wave numbers—and the active ν_1 band [24]. The absorption ν_3 band in hemihydrate splits into three bands between 1050 and 1250 cm^{-1}, suggesting lower symmetry C_{2v} or C_1 with bidentate bonding [14]. The absorption band ν_4 of SO_4 for the new phase is split, in which the presence of both monodentately bounded SO_4, typical for namuwite, and bidentately bounded SO_4 can be observed, which is presented in the hemihydrate (Figure 5).

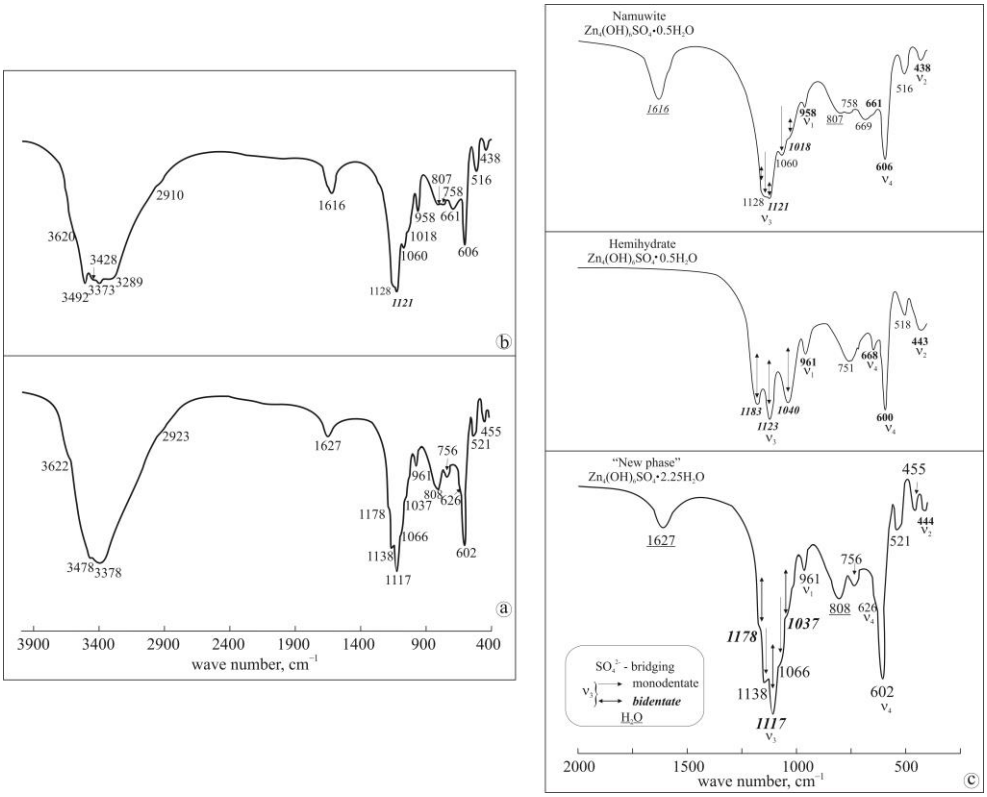

Figure 5. FTIR spectra: (**a**) new phase, (**b**) namuwite; (**c**) comparison of the SO_4 absorption bands of the new phase, namuwite, and hemihydrate.

Based on the abovementioned suggestions, the preservation and construction of the symmetry (SG P-3) of the structure with alternating namuwite and hemihydrate packages, and with unit cell parameters of a = 8.33 Å and c = 17.84 Å, was performed using the VESTA program [25] (Figure 6).

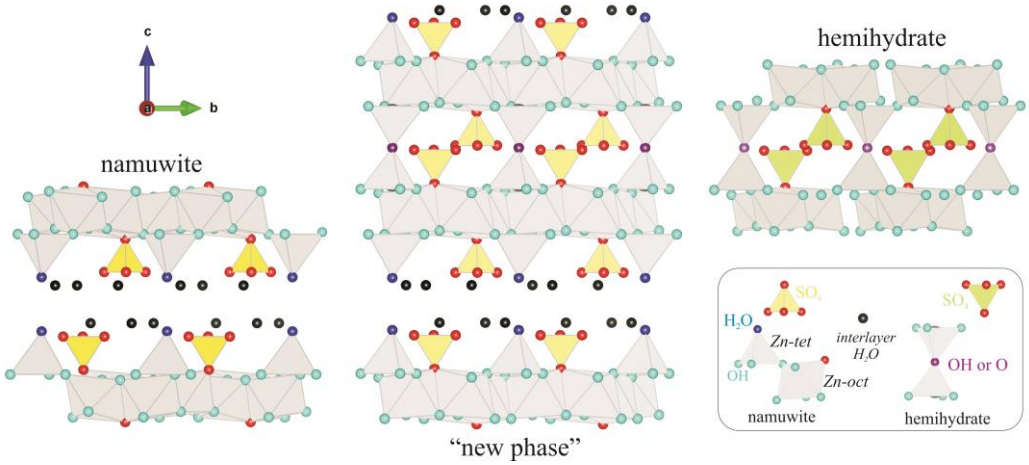

Figure 6. Schemes of crystal structures of the new phase, namuwite, and hemihydrate.

The generated powder XRD pattern from the obtained structural data using the PowderCell program [26] showed an encouragingly good fit with the experimentally obtained powder XRD pattern of the "new phase" (Figure 7).

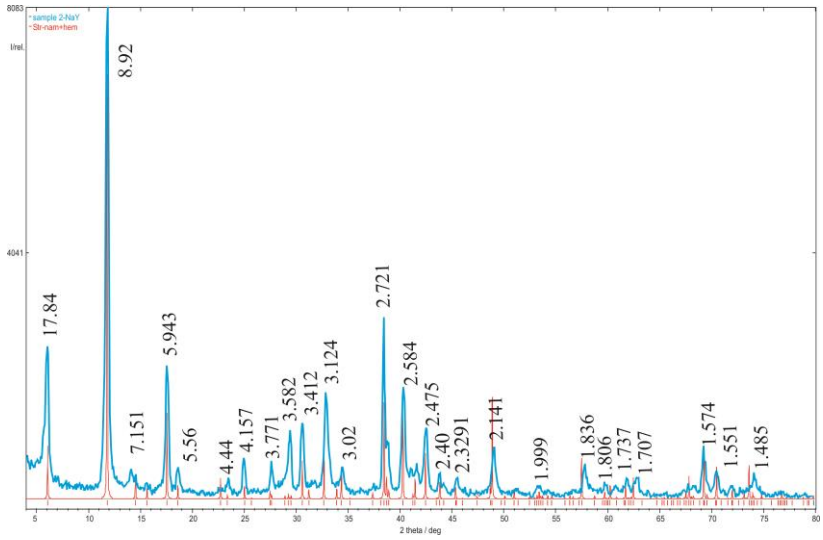

Figure 7. Powder XRD patterns of the new phase: experimental pattern (blue) and simulated pattern of the derivate structural model with lattice parameters of $\boldsymbol{a}$ = 8.333 Å, $\mathbf{c}$ = 17.84 Å, $\boldsymbol{\alpha}$ = 90°, $\boldsymbol{\beta}$ = 90°, and $\boldsymbol{\gamma}$ = 120.

3.2. Structure Refinement and Description

To verify the derived structure model, size-appropriate crystals were selected for the analysis by single-crystal diffraction methods. Single crystals (colorless, slightly cloudy, hexagonal crystals with dimensions of 0.01 × 0.05 × 0.1 mm^3, (Figure 8)) from the studied sample were carefully selected and mounted on a glass capillary. The crystals from the starting namuwite material were 50 to 150 μm in diameter. They are observed as plate crystals with a trigonal or hexagonal shape, in accordance with the trigonal symmetry of namuwite (Figure 8a,b). Crystals of the newly formed phase obtained from the parent namuwite crystals after the reaction with NaI retain the general shape and size of the parent namuwite crystals, but appear to be composed of very thin layers. The observed features can be due to either the pseudomorphosis or delamination of the parent namuwite crystals (Figure 8c,d).

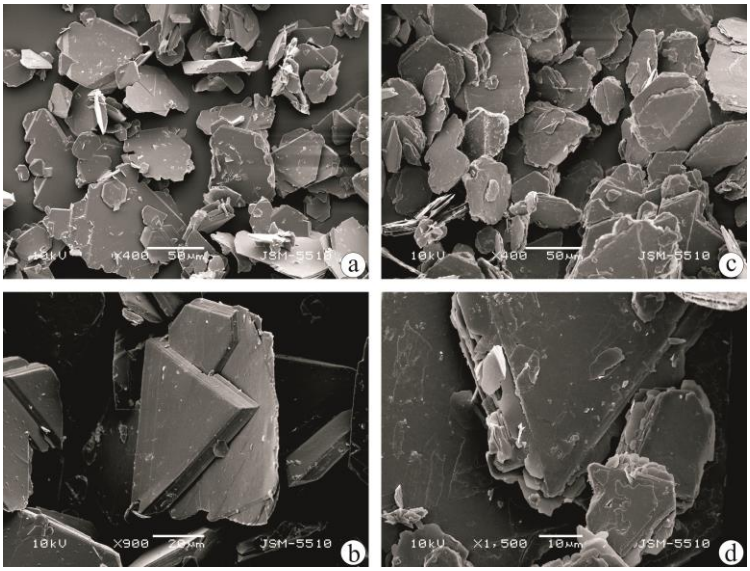

Figure 8. SEM photographs of: (**a**,**b**) the initial namuwite; (**c**,**d**) the "new phase" obtained from namuwite.

The studied sample was analyzed by a single-crystal diffraction method using a SuperNova Dual-Wavelength (Rigaku) single-crystal diffractometer. The data collection and data reduction were performed by CrysAlisPro, Rigaku Oxford Diffraction, 2017, version 1.1.171.37.35 [27]. The crystal structure was solved by direct methods using ShelxS and refined by the full-matrix least-squares method on F^2 with ShelxL (2014) programs [28,29]. All of the nonhydrogen atom positions were located successfully from difference Fourier maps. The structure determination revealed that the studied sample is built of doubled $[Zn_4(SO_4)_2(OH)_6]$ namuwite-type octahedral layers and water molecules. It was not possible to locate the hydrogen atoms of the OH groups, and the number of hydrogens in the chemical formula were added to balance the negative charge. The obtained structural model contained an additional Zn atom, indicating the presence of 7% of $Zn_2(SO_4)(OH)_6$-type layers within the studied sample. The structural model was first refined with isotropic temperature factors. Finally, the anisotropic displacement parameters of the nonoxygen atoms were refined. Selected crystal data and structure-refinement parameters are listed in Table 2. The fractional atomic coordinates are listed in Table 3.

Table 2. Crystal data and structure refinement of the new phase.

Sample	New Phase
Empirical formula/Z	$H_{15.75}\ O_{48.81}\ S_4\ Zn_{15.87}/1$
Formula weight	1962.5
Temperature/K	290(2)
Crystal system	trigonal
Space group	P-3
a/Å	8.3418(15)
b/Å	8.3418(15)
c/Å	17.595(7)
α/°	90
β/°	90
γ/°	120
Volume/Å^3	1060.3(6)

Table 2. *Cont.*

Sample	New Phase
Z	2
ϱ_{calc} g/cm^3	3.073
F(000)	946
Crystal size/mm^3	0.02 × 0.02 × 0.01
Radiation	MoKα (λ = 0.71073)
Θ range for the data collection/°	3.048 to 25.242
Index ranges	$-10 \leq h \leq 9$, $-9 \leq k \leq 10$, $-17 \leq l \leq 21$
Reflections collected	3238
Independent reflections	1482 (R_{int} = 0.0879, R_{sigma} = 0.1096)
Data/restraints/parameters	1482/0/92
Goodness-of-fit on F^2	1.604
Final R indexes (I >= 2σ (I))	R_1 = 0.1918, wR_2 = 0.4808
Final R indexes (all data)	R_1 = 0.2441, wR_2 = 0.5137
Largest diff. peak/hole/e Å^{-3}	4.742/−5.521

Table 3. Atomic coordinates, site occupancies, and equivalent isotropic displacement parameters (Å^2 × 10^3) for the studied sample.

Atom	X	Y	Z	Occupancy	U(eq)
O1	0.525(2)	0.902(2)	0.234(1)	1	23(4)
O2	0.752(2)	0.944(2)	0.3569(13)	1	34(5)
O3	0.333333	0.666667	0.367(3)	1	60(11)
O4	0.476(2)	1.101(2)	0.3462(12)	1	33(5)
O5	0.945(2)	1.192(2)	0.2271(10)	1	23(4)
O6	0.311(3)	0.481(3)	0.4887(14)	1	64(7)
O7	0.666667	1.333333	0.217(2)	1	32(8)
O8	0.825(4)	1.321(5)	0.102(2)	1	111(12)
O9	1.000	1.000	0.500	0.85	230(80)
O10	1.000	1.000	0.084(2)	0.85	89(19)
OW1	0.1049(4)	0.7070(3)	0.0570(2)	1	260(40)
S2	0.666667	1.333333	0.1311(8)	1	41(4)
S5	0.333333	0.666667	0.4594(11)	1	61(5)
Zn1	0.7145(3)	1.1319(4)	0.2989(2)	1	33(16)
Zn2	0.5801(4)	0.7135(3)	0.2930(2)	1	34(17)
Zn3	1.000	0.3954(4)	0.024(2)	0.85	26(2)
Zn4	1.000	0.1976(4)	0.031(2)	0.85	34(2)
Zn	1.000	0.294	0.069(18)	0.07	15(20)

The unit cell parameters obtained were compared with those of the minerals namuwite and hemihydrate (Table 4). While the ***a*** parameter is similar, the ***c*** parameter could be considered as the sum of the c parameters of namuwite and hemihydrate.

Table 4. Unit cell parameters of namuwite, hemihydrate, and the "new phase".

Crystal Phase	Formula	SG	Unit Cell Parameters					
			a	*b*	*c*	α	β	γ
Namuwite	$Zn_4(OH)_6SO_4.4H_2O$ (1)	P-3	8.330	8.330	10.540	90	90	120
Hemihydrate	$Zn_4(OH)_6SO_4.0.5H_2O$ (2)	P-3	8.356	8.357	7.084	90	90	120
New phase	$Zn_4(OH)_6SO_4 \cdot 2–2.25H_2O$	P-3	8.3418	8.3418	17.595	90	90	120

Unit sell parameters according to: (1) [18]; (2) [12].

The crystal structure of the sample analyzed has a P-3 trigonal symmetry. The zinc atoms occupy five crystallographic positions, two of which, Zn1 and Zn2, are fully occupied, while Zn3, Zn4, and Zn are partially occupied. The corresponding oxygen atoms are also partially occupied to maintain the logic of the structural model. Zn1, Zn2, and Zn form octahedra, while the remaining two zinc atoms have tetrahedral environments. The zinc polyhedra form doubled $[Zn_4(SO_4)_2(OH)_6]$ namuwite-type layers parallel to (110), alternating along the c-axis, with water molecules between them, most likely stabilizing the structure by forming hydrogen bonds.

The obtained structure (Figure 9a) is very similar to the deduced structural model (Figure 6), and the specified positions provide information about the specifics of the paired ("hemihydrate" type) hydroxide layer.

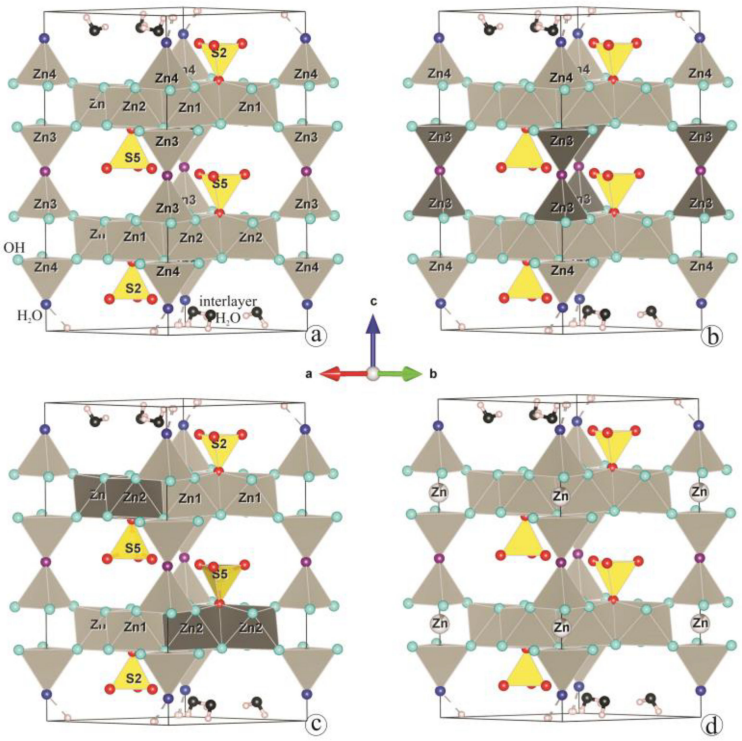

Figure 9. Crystal structure of new phase: (**a**) all obtained cation positions; (**b**) distribution of the two different Zn tetrahedra; (**c**) distribution of the two different Zn octahedra; (**d**) Zn position because of crystal defects.

According to the structural refinement in the Zn tetrahedra, three of the oxygens are from OH groups, and the apical position of the tetrahedron is different for the two zinc cations. In the Zn4 tetrahedron, the apical position is occupied by an H_2O molecule, while in the Zn3 tetrahedron, the apical position is shared with the Zn3 tetrahedron from the adjacent layer, and most likely occupied by O^{2-}. The difference in the composition and surroundings of the tetrahedra affects the bond lengths and their distortion degree (Table 5). The quantitative value of the influence of the ligand impact on the cation polyhedra can

be provided by the distortion index, D, which is based on bond lengths, and was defined by [30] as

$$D = \frac{1}{n}\sum_{i=1}^{n}\frac{|l_i - l_{av}|}{l_{av}} \quad (1)$$

where l_i is the distance from the central atom to the i^{th} coordinating atom and l_{av} is the average bond length [25].

Table 5. Bond lengths (Å) and distortion index (DI) of the polyhedra in the new phase structure.

	Bond	Zn tetrahedron	DI	Bond	Zn octahedron	DI	Bond	SO_4	DI
New phase	Zn3–O2 Zn3–O9	3 × 1.998 1.843	0.0301	Zn2–O4 Zn2–O2 Zn2–O5 Zn2–O1 Zn2–O1 Zn2–O3	2.027 2.064 2.107 2.120 2.128 2.301	0.0282	S5–O6 S5–O3	3 × 1.552 1.631	0.0175
	Zn4–O5 Zn4–O10	3 × 1.941 2.001	0.0105	Zn1–O4 Zn1–O2 Zn1–O1 Zn1–O4 Zn1–O5 Zn1–O7	2.011 2.024 2.107 2.052 2.141 2.392	0.0459	S2–O8 S2–O7	3 × 1.471 1.511	0.0112
Namuwite *	Zn1–OH2 Zn1–Wat1	3 × 1.954 1.947	0.0014	Zn2–OH1 Zn2–OH1 Zn2–OH1 Zn2–OH2 Zn2–OH2 Zn2–O1	2.018 2.052 2.055 2.097 2.159 2.431	0.0499	S–O2 S–O1	3 × 1.458 1.411	0.0120

* Data according to [15].

The Zn4 tetrahedra are more strongly deformed. The sharing of one oxygen atom located in an apical position by two tetrahedra from adjacent layers causes a contraction of the tetrahedron in the direction perpendicular to the layer and an increase in the distances between the Zn and OH groups. The Zn3 tetrahedron positioned on the opposite side of the octahedral vacancy experiences the opposite type of deformation, which is much less pronounced (Table 5). A similar tendency in the changes in the distances and degrees of distortion is observed for the Zn octahedra and sulfate tetrahedra. The zinc octahedra (Zn1), in which the associated SO_4 group (S2 tetrahedra) interacts with interlayer water molecules, show distances and and a distortion index (DI) inherent to the namuwite structure. The Zn octahedra (Zn2) and associated sulfate tetrahedra (S5) located in the space between the diortho-bonded Zn3 tetrahedrons experience different deformations caused by the environment (Figure 9c, Table 5).

Probably due to an imperfection caused either by delamination (Figure 8b), and following layer disorder, or by the presence of an interlayer with a schulenbergite-type octahedral layer, a density is observed in the vacant octahedral position (marked in Table 3 as Zn), which determines the position occupancy from 5 to 9% in various samples (Figure 9d). For this reason, the resulting R-factor is not particularly satisfactory. Despite refinement difficulties because of the bad quality of the crystals, the number of measured crystals shows similar lattice parameters and space groups, and the same structural topology. The data for the crystal with the best balance for all crystallographic parameters are deposited in the Cambridge Crystallographic Data Centre, no. CSD 1939856.

Based on the obtained detailed data, the structure of the $Zn_4(OH)_6SO_4{\cdot}2–2.25H_2O$ phase can be described as an alternation of a paired octahedral–tetrahedral doubly decorated hydroxide layer with cationic vacancies and an aqueous interlayer.

4. Conclusions

A theoretical model for the structure of the newly obtained phase $Zn_4(OH)_6SO_4{\cdot}2–2.25H_2O$ based on the crystal–chemical features and crystal structures of namuwite and hemihydrate was derived. The proposed structural model was confirmed by single-crystal structural analyses. The determined positions of the Zn cations (two octahedral

and two tetrahedral) and S (two positions) and O atoms represent the structure of the $Zn_4(OH)_6SO_4 \cdot 2–2.25H_2O$ as alternation of a paired octahedral–tetrahedral doubly decorated hydroxide layer with cationic vacancies and an aqueous interlayer. The single XRD data determined the structure with a trigonal symmetry SG of P-3, a unit cell with a = 8.3418(15) Å and c = 17.595(7) Å, and a cell volume of 1060.3(6) $Å^3$, with Z = 2.

Author Contributions: Conceptualization, T.S.; methodology, T.S., R.N., and N.P.; software, R.N.; writing—original draft preparation, T.S.; writing—review and editing, R.N. and N.P. All authors have read and agreed to the published version of the manuscript.

Funding: The Operational program "Science and Education for Smart Growth" 2014–2020 of the Ministry of Education and Science, Republic of Bulgaria, co-funded by the European Union through the European structural and Investment funds (ESI Funds).

Data Availability Statement: The crystal data are deposited in the Cambridge Crystallographic Data Centre, no. CSD 1939856.

Acknowledgments: The authors offer thanks for the technical support to the project CoE "National Center of Mechatronics and Clean Technologies", BG05M2OP001-1.001-0008-C01 and the project BG05M2OP001-1.002-0019: Clean & Circle, financed by the Operational program "Science and Education for Smart Growth" 2014–2020 of the Ministry of Education and Science, Republic of Bulgaria, cofunded by the European Union through the European structural and Investment funds (ESI Funds).

Conflicts of Interest: The authors declare no conflicts of interest.

References

1. Hawthorne, F.C.; Schindler, M. Understanding the weakly bonded constituents in oxysalt minerals. *Z. Krist.* **2008**, *223*, 41–68. [CrossRef]
2. Stanimirova, T. Crystal chemical preconditions for the species diversity of minerals-hydroxy-salts. *Geoscience* **2017**, *78*, 35–36.
3. Carbajal Arizaga, G.G.; Satyanarayana, K.G.; Wypych, F. Layered hydroxide salts: Synthesis, properties and potential applications. *Solid State Ion.* **2007**, *178*, 1143–1162. [CrossRef]
4. Maruyama, S.A.; Krause, F.; Tavares Filho, S.R.; Leitão, A.A.; Wypych, F. Synthesis, cation exchange and dehydration/rehydration of sodium gordaite: $NaZn_4(OH)_6(SO_4)Cl \cdot 6H_2O$. *Appl. Clay Sci.* **2017**, *146*, 100–105. [CrossRef]
5. Stanimirova, T. Exchange reactions of zinc hydroxide-sulfate minerals in halide solutions. *Appl. Clay Sci.* **2019**, *168*, 396–408. [CrossRef]
6. Leal, D.A.; Silva, G.M.; Tedim, J.; Wypych, F.; Marino, C.E.B. Synthesis and characterization of gordaite, osakaite and simonkolleite by different methods: Comparison, phase interconversion, and potential corrosion protection applications. *J. Solid State Chem.* **2020**, *291*, 121595. [CrossRef]
7. Nakagaki, S.; Machado, G.S.; Stival, J.F.; dos Santos, E.H.; Silva, G.M.; Wypych, F. Natural and synthetic layered hydroxide salts (LHS): Recent advances and application perspectives emphasizing catalysis. *Prog. Solid State Chem.* **2021**, *64*, 100335. [CrossRef]
8. Silva, G.M.; Wypych, F. A novel and facile synthesis route for obtaining highly crystalline impurity free layered hydroxide sulfates: Gordaite and osakaite. *Inorg. Chem. Commun.* **2022**, *143*, 109723. [CrossRef]
9. Stanimirova, T.; Delcheva, Z.; Petrova, N. New phase obtained at mutual transformations of zinc hydroxy-salts. *Bulg. Chem. Commun.* **2018**, *50*, 63–72.
10. Maruyama, S.A.; Molgero Westrup, K.C.; Nakagaki, S.; Wypych, F. Immobilization of a cationic manganese (III) porphyrin on lithium gordaite ($LiZn_4(OH)_6(SO_4)Cl \cdot 6H_2O$), a layered hydroxide salt with cation exchange capacity. *Appl. Clay Sci.* **2017**, *139*, 108–111. [CrossRef]
11. Bear, I.J.; Gray, I.E.; Madsen, I.C.; Newnham, I.E.; Rogers, L.J. Structures of basic zinc sulfates $3Zn(OH)_2 \cdot ZnSO_4 \cdot mH_2O$, m = 3 and 5. *Acta Crystallogr.* **1986**, *B42*, 32–39. [CrossRef]
12. Bear, I.J.; Gray, I.E.; Madsen, I.C.; Newnham, I.E.; Rogers, L.J. The $ZnSO_4 \cdot 3Zn(OH)_2 \cdot H_2O$ system. I. Phase formation. *Aust. J. Chem.* **1987**, *40*, 539–556. [CrossRef]
13. Moezzi, A.; Cortie, M.B.; McDonagh, A.M. Zinc hydroxide sulfate and its transformation to crystalline zinc oxide. *Dalton Trans.* **2013**, *42*, 14432–14437. [CrossRef]
14. Stanimirova, T.; Kerestedjian, T.; Kirov, G. Dehydration and rehydration of Zn-hydroxy sulfate minerals with interrupted decorated hydroxide sheets. *Appl. Clay Sci.* **2017**, *135*, 16–26. [CrossRef]
15. Groat, L.A. The crystal structure of namuwite, a mineral with Zn in tetrahedral and octahedral coordination, and its relationship to synthetic basic zinc sulfates. *Am. Mineral.* **1996**, *81*, 238–243. [CrossRef]
16. Adiwidjaja, G.; Frise, K.; Klaska, K.-H.; Schlüter, J. The crystal structure of gordaite. $NaZn_4(SO_4)(OH)_6Cl \cdot 6H_2O$. *Z. Krist* **1997**, *212*, 704–707.

17. Burns, P.C.; Roberts, A.C.; Nikischer, A.J. The crystal structure of $Ca[Zn_8(SO_4)_2(OH)_{12}Cl_2](H_2O)_9$, a new phase from slag dumps at Val Varena, Italy. *Eur. J. Mineral.* **1998**, *10*, 923–930. [CrossRef]
18. Ohnishi, M.; Kusachi, I.; Kobayashi, S. Osakaite, $Zn_4SO_4(OH)_6{\cdot}5H_2O$, a new mineral fromthe Hiraomine, Osaka, Japan. *Can. Mineral.* **2007**, *45*, 1511–1517. [CrossRef]
19. Chukanov, N.V.; Rastsvetaeva, R.K.; Aksenov, S.M.; Pekov, I.V.; Belakovskiy, D.I.; Blass, G.; Möhn, G. Lahnsteinite, $Zn_4(SO_4)(OH)_6{\cdot}3H_2O$, a new mineral from the Friedrichssegen Mine, Germany. *Geol. Ore Depos.* **2013**, *55*, 663–668. [CrossRef]
20. Bevins, R.E.; Turgoose, S.; Williams, P.A. Namuwite, $(Zn,Cu)_4SO_4(OH)_6{\cdot}4H_2O$, a new mineral from Wels. *Mineral. Mag.* **1982**, *46*, 51–54. [CrossRef]
21. Drits, V.A.; Sokolova, T.N.; Sokolova, G.V.; Cherkashin, V.I. New Members of the Hydrotalcite-Manasseite Group. *Clays Clay Miner.* **1987**, *35*, 401–417. [CrossRef]
22. Giester, G.; Rieck, B. Bechererite, $(Zn,Cu)_6Zn_2(OH)_{13}[(S,Si)(O,OH)_4]_2$, a novel mineral species from the Tonopah-Belmont mine, Arizonia. *Am. Mineral.* **1996**, *81*, 244–248. [CrossRef]
23. Hoffmann, C.; Armbruster, T.; Giester, G. The acentric structure (P3) of bechererite, $Zn_7Cu(OH)_{13}[SiO(OH)_3SO_4]$. *Am. Mineral.* **1997**, *82*, 1014–1018. [CrossRef]
24. Nakamoto, K. *Infrared and Raman Spectra of Inorganic and Coordination Compounds*; Wiley: New York, NY, USA, 1986.
25. Momma, K.; Izumi, F. VESTA 3 for three dimensional visualization of crystal, volumetric and morphology data. *J. Appl. Crystallogr.* **2011**, *44*, 1272–1276. [CrossRef]
26. Kraus, W.; Nolze, C. POWDER CELL—A program for the representation and manipulation of crystal structure and calculation of the resulting X-ray powder pattern. *J. Appl. Crystallogr.* **1996**, *29*, 301–303. [CrossRef]
27. CrysAlis Pro. *Agilent Technologies*; UK Ltd.: Yarnton, UK, 2011.
28. Sheldrick, G. A short history of SHELX. *Acta Crystallogr. A* **2008**, *64*, 112–122. [CrossRef] [PubMed]
29. Sheldrick, G. Crystal structure refinement with SHELXL. *Acta Crystallogr. C* **2015**, *71*, 3–8. [CrossRef]
30. Baur, W.H. The geometry of polyhedral distortions. Predictive relationships for the phosphate group. *Acta Crystallogr. B* **1974**, *30*, 1195–1215. [CrossRef]